Photoinduced Intramolecular Charge Transfer: Photodissociation of CO_2^+·Ar Cluster Ions

Andreas J. Illies,† Martin F. Jarrold, Winfried Wagner-Redeker, and Michael T. Bowers*

Contribution from the Department of Chemistry, University of California, Santa Barbara, Santa Barbara, California 93106. *Received September 24, 1984*

Abstract: Photon absorption by CO_2^+·Ar in the visible wavelength range results in intramolecular charge transfer to form CO_2·Ar^{+*}. The observed photodissociation product ions are Ar^+ and CO_2^+. Limits on the lifetime of the CO_2·Ar^{+*} ion are determined from the angular dependence of the photodissociation product peaks. The lifetime of CO_2·Ar^{+*} ion resulting in Ar^+ formation is shown to dramatically decrease as product velocity increases. The Ar^+ photofragment is formed by two processes: vibrational predissociation of a bound CO_2·Ar^+ cluster and direct dissociation from a CO_2·Ar^+ repulsive state. The latter process leads to formation of CO_2 photofragments in which the v_1 symmetric stretch appears to be excited. The results suggest that the CO_2 fragment has little rotational energy, suggesting a T-shaped or linear CO_2^+·Ar cluster structure. The CO_2^+ photofragment comes from a CO_2·Ar^{+*} photoexcited complex whose lifetime is longer than a rotational period, probably via electronic predissociation of a bound state of CO_2·Ar^{+*}. The total photodestruction cross section remains relatively constant at approximately 1.1×10^{-17} cm^2 from 514 to 458 nm while the percent CO_2^+ product ion formed decreases from 14% to 5.5% over the same wavelength range. At least two bound and two repulsive surfaces are involved in the system. These surfaces and the detailed dissociation dynamics are discussed.

Weakly bound ion–molecules clusters are species that can be thought of as being similar to a collision complex.[1] The collision complex is a quasimolecule corresponding to a configuration of a reacting system which is intermediate between reactants and products. Unfortunately, since the collision complex is usually a transitory species, direct experimental observation of such quasimolecules has been extremely difficult. Recently, however, experiments have been designed to directly observe properties of such transitory species.[2-4] In those experiments, laser irradiation affects the outcome of a collision event even though the laser field is *not* resonant with the stable separated collision partners. Thus, irradiation of an intermediate quasimolecule or transition state is postulated.

In the present work we report on the photodissociation of CO_2^+·Ar cluster ions. Studies of ion–molecule cluster ions are important in their own right due to their abundance in the earth's upper atmosphere and the role they play in solvation and vapor-to-liquid transitions.[5-8] Ion–molecule clusters are also of fundamental interest because their bonding is intermediate between van der Waals molecules and covalent bonds and because they are often intermediates in bimolecular ion–molecule reactions.[9]

Photodissociation of the CO_2^+·Ar cluster ion is important for at least three reasons. First, it is of fundamental interest and, as will be shown, the photodissociation dynamics of CO_2^+·Ar involves at least three dissociation pathways and four potential surfaces. The second reason is the similarity between the CO_2^+·Ar and CO_2·Ar^+ ion–molecule clusters and "transient" collision complexes. Third, photodissociation of CO_2^+·Ar relates to the bimolecular charge-transfer reaction between Ar^+ and CO_2:

$$Ar^+ + CO_2 \rightarrow CO_2\cdot Ar^{+*} \quad (1a)$$

$$CO_2\cdot Ar^{+*} \rightarrow CO_2^+ + Ar \quad (1b)$$

$$\rightarrow Ar^+ + CO_2 \quad (1c)$$

In our photodissociation studies, the reactant is the CO_2^+·Ar cluster ion. Upon absorption of a photon, an excited state of the cluster ion is produced which is similar to the collision complex in reaction 1. For example,

$$CO_2^+\cdot Ar + h\nu \rightarrow CO_2\cdot Ar^{+*} \quad (2a)$$

$$CO_2\cdot Ar^{+*} \rightarrow CO_2^+ + Ar \quad (2b)$$

$$\rightarrow Ar^+ + CO_2 \quad (2c)$$

Reactions of this type (reaction 2) are often referred to as "half collisions".[10] Note that reaction 2a has been written as an intramolecular charge-transfer reaction; the reasons for this are made clear later in this paper.

Dissociation of the CO_2·Ar^{+*} complex in reactions 1 and 2 is expected to be similar if the same electronic surfaces are involved. In the charge-transfer reaction, the branching between reactions 1b and 1c determines the bimolecular rate constant relative to the collision rate for reaction 1a. In the photodissociation, the rate constants for reactions 2b and 2c determine the photodissociation branching ratio. The advantages of using photoexcitation are that the angular momentum distribution is controlled (if the reactant CO_2^+·Ar ions can be thermalized), the initial geometry of the excited state is well-defined (it is the same as that of the reactant cluster ion[11]), and the excitation energy can be controlled by varying the photon energy.[11] The collision complex can therefore be prepared with varying amounts of internal energy and can be controlled more easily in photodissociation experiments than in bimolecular reactions.

† Permanent address: Department of Chemistry, Auburn University, Auburn, AL 36849.

(1) The terms "transition state" and "activated complex" are closely related and refer to a quasimolecule which is intermediate between reactants and products. In ion–molecule reactions there also often exists a "collision complex" which is a long-lived species in a potential well. This "collision complex" arises from the attractive ion-induced dipole potential in the ion–molecule encounter. The "collision complex" can be relatively long-lived (10^{-12}–10^{-9} s) for small systems, such as those considered in this paper.

(2) Brooks, P. R.; Curl, R. F.; Maguire, T. C. *Ber. Bunsenges. Phys. Chem.* **1982**, *86*, 401. Hering, P.; Brooks, P. R.; Carl, R. F.; Judson, R. S.; Lowe, R. S. *Phys. Rev. Lett.* **1980**, *44*, 687.

(3) Wilcomb, B. E.; Burnham, R. E. *J. Chem. Phys.* **1981**, *74*, 6784.

(4) Jouvet, C.; Svep, B. *Chem. Phys. Lett.* **1983**, *96*, 436. Ono, Y.; Ng, C. Y. *J. Chem. Phys.* **1982**, *77*, 2947.

(5) Ferguson, E. E.; Fehsenfeld, F. C.; Albritton, D. L. In "Gas Phase Ion Chemistry"; Bowers, M. T., Ed.; Academic Press: New York, 1979; Vol. 1, pp 45–82.

(6) Kebarle, P. *Annu. Rev. Phys. Chem.* **1977**, *28*, 445.

(7) Castleman, A. W. In "Kinetics of Ion-Molecule Reactions"; Ausloos, P., Ed.; Plenum: New York, 1979; pp 295–321. Castleman, A. W. *Adv. Colloid Interface Sci.* **1979**, *10*, 73.

(8) Mark, T. D.; Castleman, A. W. *Adv. At. Mol. Phys.*, in press.

(9) Maut-Ner, M. In "Gas Phase Ion Chemistry"; Bowers, M. T.; Ed.; Academic Press: New York, 1979.

(10) For a recent critical review of photodissociation see: Simons, J. P. *J. Phys. Chem.* **1984**, *88*, 1287.

(11) The absorption of a photon occurs on a very rapid time scale compared to the collision time between two molecules and compared to nuclear motions. The initial geometry of the excited state will therefore resemble that for the ground state. The internal energy distribution of the excited state is determined by the internal energy of the ground-state cluster ion and the transition probabilities.

0002-7863/85/1507-2842$01.50/0

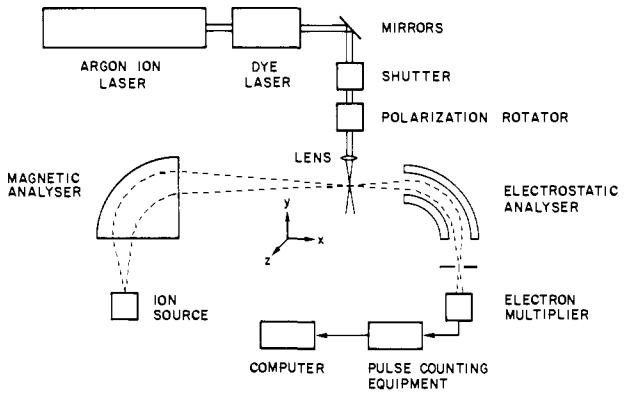

Figure 1. Schematic diagram of the instrument.

In this paper we report the photodissociation product kinetic energy release distributions, the photodissociation branching ratios, total photodissociation cross sections, and estimates of the lifetime of the photoexcited state. The potential surfaces for the system are discussed and used to interpret the photodissociation and charge-transfer reaction dynamics.

Experimental Section

The experimental apparatus is schematically shown in Figure 1. The experiment and techniques have been described in detail elsewhere[12,13] and therefore will only be briefly reviewed here. The apparatus consists of a reverse geometry mass spectrometer (V. G. Analytical, ZAB 2F), an argon ion laser (Coherent Innova 20), and a dye laser (Coherent 599). The CO_2^+·Ar cluster ions were formed by ion–molecule reactions in a high-pressure ion source constructed at UCSB which was cooled to ~200 K by flowing cold nitrogen gas through a channel in the copper source block.[14] The electron energy was 150 eV, and the ion extraction potential was 0 V. The ion source pressure was 0.10–0.12 torr as measured with an MKS Baratron capacitance manometer. The ions exited the ion source through a 0.64 mm × 4 mm slit, were accelerated to 8 kV, and were mass analyzed by the magnet. The mass selected ion beam was brought to a spatial focus in the second field free region of the mass spectrometer and crossed with a focused laser beam. The ionic products resulting from photodissociation were mass and energy analyzed by scanning the electrostatic analyzer (ESA) at a resolving power of ~2500 (fwhm). The laser beam was modulated by using a shutter, and up-down counting was used to subtract any background product ions formed by collision-induced dissociation or unimolecular "metastable" dissociation. The laser polarization was rotated with a Spectra Physics 310A polarization rotator. For reasons to be made clear in the Results and Discussion section, angles of 0°, 54.7°, and 90° relative to the ion beam direction were used. Ions were detected by using an 18-stage venetian blind electron multiplier. The data were accumulated in a multichannel analyzer (MCA) which was slaved to scan synchronously with the ESA voltage. The data were transferred from the MCA to a PDP 11/34 computer for analysis. The gases were from Matheson (Ar, 99.995%; CO_2, 99.8%) and were used without further purification.

Formation of CO_2^+·Ar Cluster Ions. CO_2^+·Ar was generated in the ion source under chemical ionization conditions by using a mixture of mostly Ar with a trace amount of CO_2 (approximately 0.1%) at a total ion source pressure between 0.10 and 0.12 torr. Under these conditions the primary processes which occur are electron impact of Ar followed by rapid charge transfer to form CO_2^+; the charge-transfer reaction occurs at approximately 50% of the collision rate for near thermal reactants.[15,16] The CO_2^+ ions then undergo ion–molecule association reactions with neutral Ar and CO_2, resulting in CO_2^+·Ar and CO_2·CO_2^+. These ion–molecule clusters then undergo a series of "ligand" switching reactions. The switching reaction

$$CO_2^+\cdot Ar + CO_2 \rightarrow CO_2\cdot CO_2^+ + Ar \qquad (3)$$

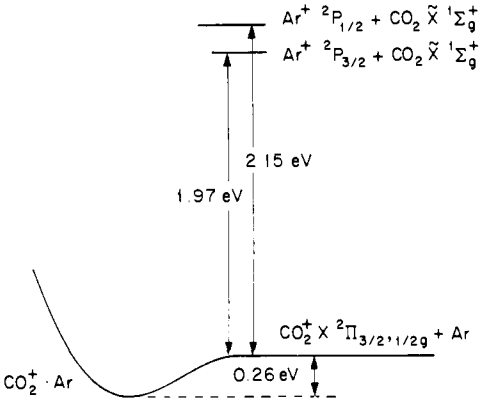

Figure 2. Diagram showing the known thermodynamic quantities for the CO_2^+·Ar system.

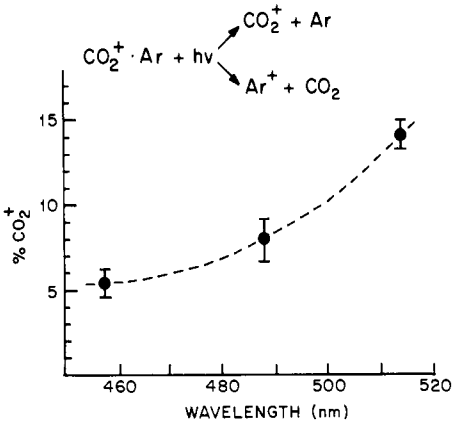

Figure 3. Plot of the branching ratio $100[iCO_2^+/i(CO_2^+ + iAr^+)]$ against the photon energy.

is exothermic by 0.435 eV and probably very fast.[17] In order to avoid this depletion reaction, the CO_2 neutral concentration had to be kept very low. The consequence of such a low CO_2 concentration was that the CO_2^+·Ar cluster ion intensity was very low. The photodissociation product signals were therefore extremely weak (typically 10–200 counts/s on the peak maximum depending upon the laser power, photon wavelength, and ion source conditions).

Results and Discussion

Both Ar^+ and CO_2^+ product ions were observed upon photodissociation of CO_2^+·Ar between 458 and 514 nm. Figure 2 shows a potential diagram which depicts the known energetics for this system. Note that the reaction between CO_2^+ and Ar correlates with the CO_2^+·Ar cluster ion where the charge is localized on CO_2. The bond dissociation energy of CO_2^+·Ar has been measured to be 0.26 eV.[18] The reaction between Ar^+ and CO_2 must initially correlate with a different cluster ion, presumably CO_2·Ar^+, where the charge is localized on Ar. The bond dissociation energy of CO_2·Ar^+ is, to our knowledge, not known. With the photon energies employed in these experiments, no other products are energetically accessible from ground-state CO_2^+·Ar cluster ions.

Photodissociation Branching Ratios and Total Cross Sections. Photodissociation branching ratios can easily be determined with our apparatus and are useful in the interpretation of fragmentation dynamics. We performed relative measurements of the Ar^+ and CO_2^+ photodissociation product ions by integrating over the product peaks. The experimental intensities were corrected for variation of the laboratory energy resolution with product ion energy as previously described.[19]

(12) Jarrold, M. F.; Illies, A. J.; Bowers, M. T. *J. Chem. Phys.* **1983**, *79*, 6086.
(13) Jarrold, M. F.; Illies, A. J.; Bowers, M. T. *J. Chem. Phys.* **1984**, *81*, 214.
(14) Illies, A. J.; Jarrold, M. F.; Bowers, M. T. *J. Am. Chem. Soc.* **1982**, *104*, 3587.
(15) (a) Fehsenfeld, F. C.; Ferguson, E. E.; Schmeltekopf, A. L. *J. Chem. Phys.* **1966**, *45*, 404. (b) Kemper, P. R.; Bowers, M. T., unpublished results.
(16) Marx, R. In "Ionic Processes in the Gas Phase"; Almoster Ferreira, M. A., Ed.; D. Reidel: Dordrecht, Netherlands, 1982; NATO Adv. Study Inst. Ser.; p 67.
(17) Thermodynamic data were obtained from ref 18 and: Rosenstock, H. M.; Draxl, K.; Steiner, B. W.; Herron, J. T. *J. Phys. Chem. Ref. Data, Suppl.* **1977**, *6*, No. 1. (Energetics of Gaseous Ions)
(18) Pratt, S. T.; Dehmer, P. M. *J. Chem. Phys.* **1983**, *78*, 6336.
(19) Jarrold, M. F.; Illies, A. J.; Bowers, M. T. *J. Chem. Phys.* **1984**, *81*, 222.

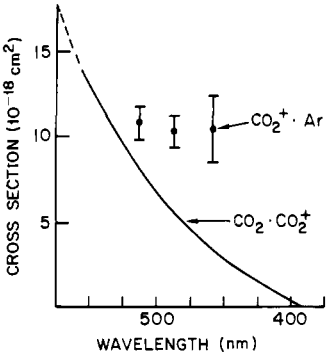

Figure 4. Total cross section for the photodissociation of $CO_2^+ \cdot Ar$ (points). The line shows the total photodissociation cross sections for $CO_2 \cdot CO_2^+$ measured by Smith and Lee (ref 20).

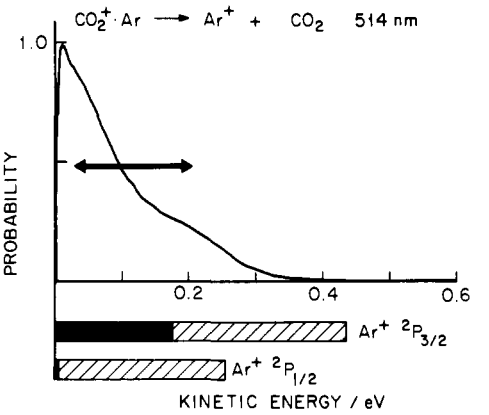

Figure 5. Ar^+ product kinetic energy release distribution for photodissociation of $CO_2^+ \cdot Ar$ at 514 nm. The double pointed arrow shows the energy separation between the two spin orbit states of Ar^+. The bar graphs below the x axis show the kinetic energy regimes accessible for ground-state $CO_2^+ \cdot Ar$ (dark regions) and internally excited $CO_2^+ \cdot Ar$ (hatched region).

The percent CO_2^+ product ion is shown in Figure 3 at the three wavelengths at which measurements were performed. Here the CO_2^+ intensity is given as a percent of the total product ion intensity. The photofragment CO_2^+ product ion decreases with increasing photon energy. This result is in qualitative agreement with charge-transfer experiments (reaction 1) which show that the $Ar^+ + CO_2$ charge-transfer rate decreases with increasing translational energy.[15] The measured charge-transfer rate is approximately 50% of the collision rate at near thermal energies. The similarities between the charge-transfer reaction and the photodissociation reaction were discussed in the introduction. We will return to this point and a more detailed analysis of the fragmentation dynamics later in this paper.

Measurement of absolute photodissociation cross sections is more difficult in our experiment because of the difficulty in determining the spatial overlap between the ion beam and the laser beam. It is, however, a simple matter to measure relative photodissociation cross sections. Smith and Lee[20] have measured reliable cross sections for photodissociation of $(CO_2)_2^+$ over the wavelength range 400–850 nm. At the ion source conditions used in our experiments, the $(CO_2)_2^+$ cluster ion was between 4 and 8 times as intense as the $CO_2^+ \cdot Ar$ cluster ion. Since both ions are present in the ion source at the same time, photodissociation of the $(CO_2)_2^+$ cluster ion was used as a reference for relative cross-section measurements of $CO_2^+ \cdot Ar$. Relative measurements were performed by integrating over the product ion peaks. The measured intensities were corrected for variation of the laboratory energy resolution with product ion energy.[19]

The resulting total photodissociation cross section between 514 and 458 nm determined by integrating over the product peaks is shown in Figure 4. The $CO_2^+ \cdot Ar$ ions may contain a small amount of excess internal energy (up to a maximum of 0.26 eV—see section on Kinetic Energy Release Distributions). The cross section for $CO_2^+ \cdot Ar$ is larger than that for $(CO_2)_2^+$ over the same wavelength range. The error bars are relatively large due to the extremely weak $CO_2^+ \cdot Ar$ parent ion intensity. At 458 nm the laser power is also weak, resulting in an even weaker product intensity and a larger error bar. No photodissociation products were observed at 610 nm. At this wavelength the laser power is approximately 5 times weaker than at 514 nm. A product ion signal which was 10 times weaker than that at 514 nm could have been detected. The cross section at 610 nm is therefore less than 5×10^{-18} cm^2.

The $CO_2^+ \cdot Ar$ photodissociation cross section is blue-shifted relative to $(CO_2)_2^+$. A red shift would be expected for a cluster with a weaker bond dissociation energy if the photodissociation occurs from a repulsive state. In the present case, however, the situation is more complex and the shift cannot be interpreted by such simple arguments.

Product Relative Kinetic Energy Release Distributions. Kinetic energy release distributions for fragmentation of molecules contain a great deal of information on the dynamics of the dissociation process.[21-27] Fragmentation from photodissociation does not occur in an isotropic manner.[28-30] However, for our experimental setup one can obtain the relative kinetic energy release distributions from experimental peak shapes collected when the laser polarization is oriented at the "magic angle", 54.7°, with respect to the ion beam direction.[13] At this angle, the experimental product ion peak is independent of the product angular distribution and only contains information on the relative kinetic energy release distribution[13] (obtained by taking the derivative of the experimental peak with respect to the laboratory energy and changing the energy axis to the center of mass scale).[27]

Figure 5 gives the kinetic energy release distribution for formation of Ar^+/CO_2 products from photodissociation of $CO_2^+ \cdot Ar$ at 514 nm. This distribution has an inflection at approximately 0.12 eV. The distribution is peaked very close to zero. Product kinetic energy release distributions which are peaked close to zero are indicative of dissociation mechanisms that do not involve a reverse activation barrier. Vibrational predissociation through an orbiting transition state is an example of such a process.[25,26] The inflection in the distribution suggests that there are two reaction paths leading to the production of Ar^+ at this photon energy. The bold double pointed arrow in Figure 5 shows the energy separation (0.178 eV) between the $^2P_{3/2}$ and the $^2P_{1/2}$ spin–orbit states of Ar^+. At first glance the data suggest that the inflection in the distribution might be due to production of both spin–orbit states of the Ar^+ ion. For reasons to be made clear

(20) Smith, G. P.; Lee, L. C. *J. Chem. Phys.* **1978**, *69*, 5393.

(21) For metastable reactions of ions we have observed and modeled kinetic energy release distributions for rotational predissociation,[14,22] electronic predissociation,[23] and vibrational predissociation through an orbiting transition state.[24,25] It is also possible to assign vibrational predissociation through a tight transition state from the kinetic energy release distributions;[25] however, metastable fragmentation through a tight transition state has not yet been modelled in our laboratory. For photodissociation in the visible wavelength range we have been able to study rapid fragmentation occurring on a repulsive surface[12,13] and slow vibrational predissociation from highly excited ground-state ions[26] using the kinetic energy release distributions as a diagnostic probe. Photodissociation of vibrationally excited ions by single infrared photon absorption has also been characterized by using the kinetic energy release distribution.[27]

(22) Jarrold, M. F.; Illies, A. J.; Bowers, M. T. *Chem. Phys. Lett.* **1983**, *92*, 653.

(23) Jarrold, M. F.; Illies, A. J.; Bowers, M. T. *Chem. Phys.* **1982**, *65*, 19.

(24) Illies, A. J.; Jarrold, M. F.; Bowers, M. T. *J. Am. Chem. Soc.* **1983**, *105*, 5775.

(25) Jarrold, M. F.; Wagner-Redeker, W.; Illies, A. J.; Kirchner, N. J.; Bowers, M. T. *Int. J. Mass Spectrom. Ion Phys.* **1984**, *58*, 63.

(26) Illies, A. J.; Jarrold, M. F.; Bowers, M. T. *J. Phys. Chem.* **1984**, *88*, 5204.

(27) Jarrold, M. F.; Illies, A. J. Kirchner, N. J.; Wagner-Redeker, W.; Bowers, M. T.; Mandich, M. L.; Beauchamp, J. L. *J. Phys. Chem.* **1983**, *87*, 2213.

(28) Zare, R. W. *Mol. Photochem.* **1972**, *4*, 1.

(29) Busch, G. E.; Wilson, K. R. *J. Chem. Phys.* **1972**, *56*, 3638.

(30) Zare, R. N.; Herschbach, D. R. *Proc. IEEE* **1963**, *51*, 173.

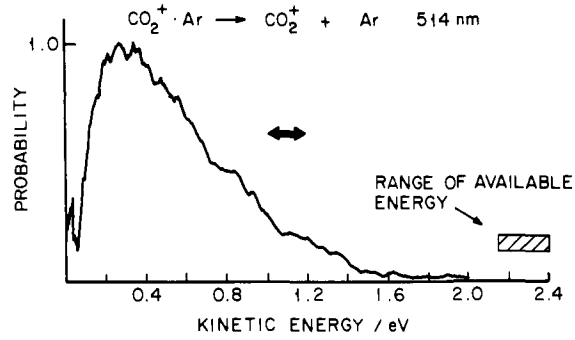

Figure 6. CO_2^+ product kinetic energy release distribution for photodissociation of CO_2^+·Ar at 514 nm. The double pointed arrow shows the energy separation between the two spin orbit states of Ar^+. The hatched bar shows the range of available energy, assuming internal excitation of CO_2^+·Ar.

later, however, vibrational excitation of the CO_2 product will be favored as the source of the inflection in the kinetic energy release distribution.

The solid dark portion of the bar graph below the kinetic energy release distribution in Figure 5 shows the kinetic energy regime which is accessible to ground-state CO_2^+·Ar cluster ions at the photon energy used.[31] The observed kinetic energy release extends farther than the total available energy for ground-state ions, which indicates that a portion of the CO_2^+·Ar cluster ions are vibrationally excited. The hatched region of the bar graph shows the additional Ar^+ kinetic energy that could result from internal energy in the CO_2^+·Ar cluster before the photon is absorbed (from the bond dissociation energy measured by Pratt and Dehmer, 0.26 eV).[18] In our experiments, the ion source pressure was high enough for some stabilizing collisions to occur. However, the CO_2^+·Ar cluster ions which survive the ligand switching reaction (reaction 3) are probably formed near the ion exit slit where the probability of exiting the source is greater than an encounter with CO_2 neutral molecule. Also argon (which was the major component of the neutral gas) is not expected to act efficiently in quenching vibrational excitation. It is thus reasonable to expect that a fraction of the CO_2^+·Ar cluster ions is vibrationally excited.

The kinetic energy release distribution for Ar^+ at 488 nm is very similar to that at 514 nm. The product average kinetic energy release at both wavelengths is the same within experimental error. The kinetic energy release distributions for Ar^+ at 458 nm are different from those at 514 and 488 nm. These distributions and the energy partitioning among the available product states are discussed later in the paper.

Figure 6 shows the kinetic energy release distribution for photodissociation of CO_2^+·Ar clusters leading to CO_2^+ + Ar fragments at 514 nm. The first and most obvious difference between the CO_2^+ and Ar^+ distributions is the magnitude of the kinetic energy release (note that Figures 5 and 6 have different energy scales). The CO_2^+/Ar products are 1.97 eV more stable than $Ar^+(^2P_{3/2})/CO_2$ products (Figure 2). This additional energy is available for partitioning into translational energy of the CO_2^+/Ar products.

The kinetic energy distribution in Figure 6 rises from zero probability slowly and peaks at a relatively large value of kinetic energy (~0.35 eV). This peak occurs between 14 and 16% of the available energy depending upon the amount of internal energy in the CO_2^+·Ar reactant cluster ion. Distributions of this sort are characteristic of fragmentation which takes place on a repulsive surface[12,13] or of vibrational predissociation through a tight transition state.[25] As will become clearer in the next sections of this paper, we suggest that the mechanism leading to formation

(31) The available energy (E_{AV}) is given by $E_{AV} = E_{h\nu} - D_0^\circ + E_{INT}$, where $E_{h\nu}$ is the photon energy, D_0° is the bond dissociation energy of the reactant cluster ion, and E_{INT} is the reactant cluster ions' initial internal energy (prior to absorption of a photon). The bond dissociation energy for CO_2^+·Ar has been measured by photoionization of the neutral van der Waals cluster to be 0.26 eV.[18]

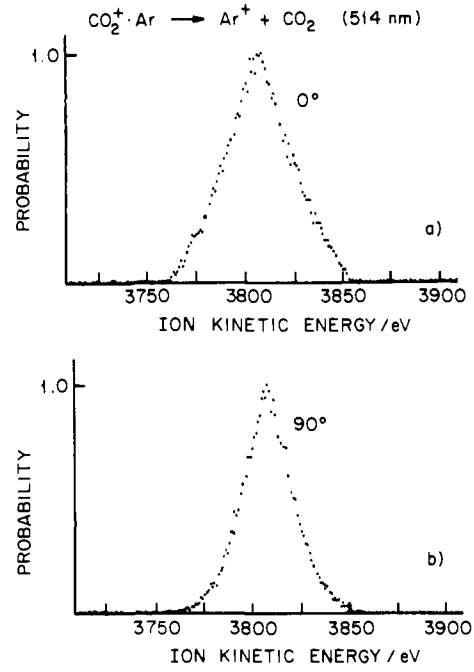

Figure 7. 514-nm photodissociation peak shapes for production of Ar^+ at 0° (a) and 90° (b) angles between the laser polarization and the ion beam direction.

of CO_2^+/Ar is electronic predissociation of CO_2·Ar^+ involving a repulsive surface.

Fragmentation Time Scales. Experimental peak shapes for photodissociation (at angles between the photon electric vector and the ion beam direction other than 54.7°) contain information on the center of mass angular distributions of the photofragments.[12,13,26] The photoproduct angular distribution has the form[28-30]

$$P(\theta) = (4\pi)^{-1}[1 + \beta P_2(\cos\theta)] \quad (4)$$

where $P(\theta)$ is the probability that the products fragment into a solid angle $d\omega$ at an angle θ with respect to the electric vector of the laser, $P_2(\cos\theta)$ is the second-degree Legendre polynomial in $\cos\theta$, and β is the asymmetry parameter. β can have values between +2 and −1.

The angular distribution depends upon the lifetime of the dissociating species. A dissociation mechanism which is rapid compared to molecular rotation results in a very anisotropic angular distribution. Different peak shapes are therefore experimentally observed when the laser electric vector is oriented at 0° and 90° with respect to the ion beam direction. These different shapes arise since the ESA measures essentially the component of kinetic energy along the ion beam direction (x direction). For a parallel transition at 0° for a dissociating state with a lifetime short relative to a rotational period, the kinetic energy is preferentially released in the x direction of the instrument (see Figure 1). A similar reaction occurring with the electric vector of the laser at 90° results in the product kinetic energy being preferentially released in the y direction. These two processes result in dramatically different peak shapes.[12,13,26] Thus, for a dissociation process rapid relative to rotational motion, varying the laser orientation will change the measured peak shape. For fragmentations slow compared to the molecular rotation time scale, rotational averaging "blurs" the angular distributions and the peak shapes at 0° and 90° become more similar.[26] Therefore, experimental peak shapes provide a crude molecular clock which operates on the rotational time scale.

Figure 7a,b shows the experimental 0° and 90° Ar^+ product peaks for photodissociation of CO_2^+·Ar clusters at 514 nm. The 0° and 90° peaks shown are nominally similar; however, the 0° peak is broader than the 90° peak. This can be easily seen near the base line where the 0° peak rises in a near linear fashion while the 90° peak is much more curved. Recently we developed a

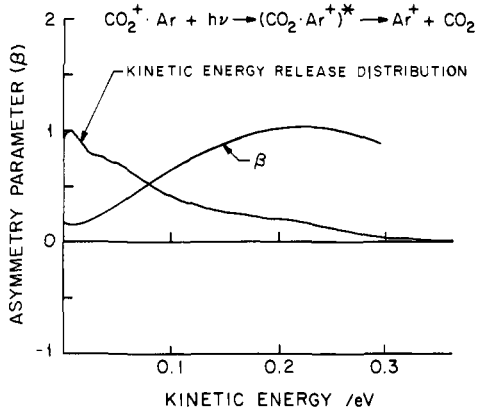

Figure 8. Plot of the asymmetry parameter β as a function of the product kinetic energy release at 514 nm (see text for more details).

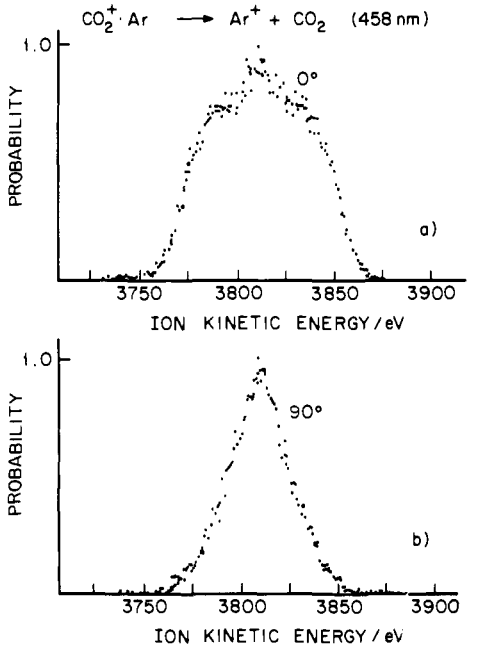

Figure 9. Peak shapes for formation of Ar^+ by photodissociation at 458 nm. The angle between the laser polarization and the ion beam direction is 0° for (a) and 90° for (b).

method to directly extract the asymmetry parameters (β) as a function of the product kinetic energy from the measured 0° and 90° peak shapes.[32] The results of this analysis are shown in Figure 8 for Ar^+ at 514 nm. Also shown in Figure 8 is the kinetic energy release distribution. The values of β at the highest and lowest energies in the plot are expected to be unreliable due to the poor signal to noise at the extremes of the kinetic energy release distribution. Figure 8 shows that, for Ar^+ photofragments, the value of β increases with increasing kinetic energy. The value of β starts at ~0.3 at low kinetic energy and fairly rapidly increases to a maximum of 1.0 at higher kinetic energy. β is a complex quantity which depends upon the orientation of the transition dipole moment, the lifetime of the excited species, and the axis along which fragmentation takes place. In general, however, values of β near zero indicate near-isotropic fragmentation and hence rotational averaging while values larger than ~0.4 indicate anisotropic angular distributions which come about from fragmentation which is rapid compared to the rotational time scale. The variation of β with product kinetic energy suggests that there may be two or more mechanisms for formation of the Ar^+ product.

The peak shapes at 458 nm for Ar^+ at 0° and 90° are shown in Figure 9. At this wavelength the 0° and 90° peaks are very

(32) Jarrold, M. F.; Illies, A. J.; Bowers, M. T. *J. Chem. Phys.* **1985**, *82*, 1832.

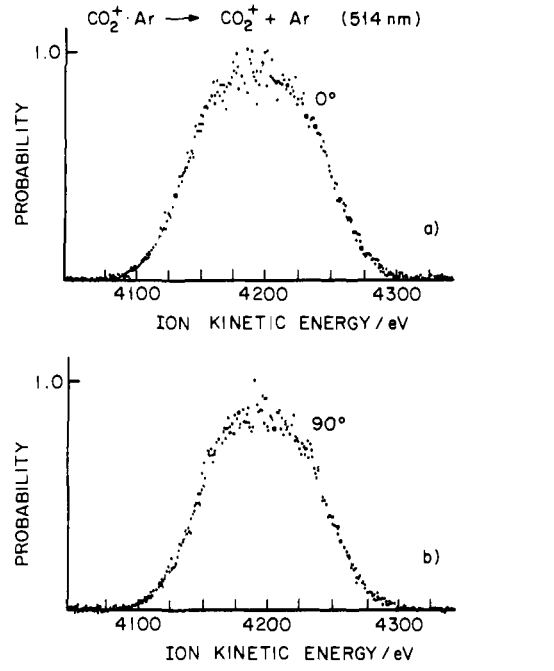

Figure 10. 514-nm photodissociation peak shapes for production of CO_2^+ at 0° (a) and 90° (b) angles between the laser polarization and the ion beam direction.

different. The peak at 0° clearly shows two components, a narrow one and a much broader one. The broader component resembles those for photodissociation from a repulsive surface. The peak at 90° does not show the different components as clearly since the peak shapes resulting from kinetic energy released in the y direction via a rapid dissociation on a repulsive surface and those for rotationally average processes are similar.[12,13,19,26]

Parts a and b of Figure 10 show the photofragment peak shapes for CO_2^+ at 514 nm for 0° and 90°, respectively. In this case the 0° and 90° peaks are very similar, which indicates that complete rotational averaging is very probable. This result suggests that fragmentation leading to CO_2^+ occurs on a time scale which is long on a rotational time scale.

Fragmentation Dynamics. From the experimental data for the photofragmentation reactions of $CO_2^+ \cdot Ar$, at least three fragmentation pathways have been identified. They are

$$CO_2^+ \cdot Ar + h\nu \rightarrow Ar^+(S) + CO_2 \quad (5a)$$

$$\rightarrow Ar^+(F) + CO_2 \quad (5b)$$

$$\rightarrow CO_2^+(S) + Ar \quad (5c)$$

(S) and (F) denote fast and slow fragmentation on the rotational time scale as indicated by the angular dependence of the experimental peak shapes. We propose that the slow step for Ar^+ formation, eq 5a, is due to vibrational predissociation (unimolecular decomposition) of $CO_2 \cdot Ar^+$. This reaction path is labeled a in Figure 11. The potential surfaces in Figure 11 are drawn by analogy to those calculated for the F/H_2 reaction system which involves the same state designations as those for Ar^+/CO_2.[33] As drawn in Figure 11, the fragmentation pathway labeled a is in direct competition with that labeled c (to be discussed) since they sample the same phase space, but it does not compete with those labeled b and b' since these take place on entirely different surfaces.

Figure 12 shows three kinetic energy release distributions for production of Ar^+. The distribution at 514 nm is the same as that in Figure 5. The distribution at 458 nm is clearly bimodal. The high energy feature of the distribution at 458 nm occurs at approximately the same energy as those at 488 and 514 nm. One possible explanation is that this higher energy feature originates

(33) Tully, J. C. *J. Chem. Phys.* **1974**, *60*, 3042.

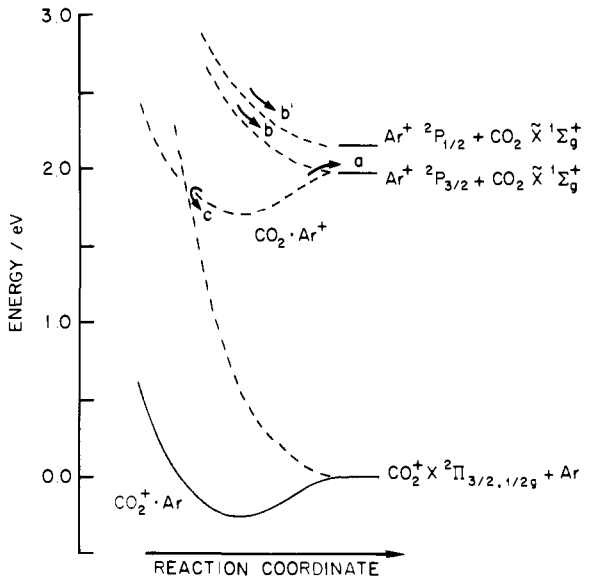

Figure 11. Schematic potential diagram showing the known energetics and the proposed fragmentation pathways for the CO_2^+·Ar cluster ion system (see text).

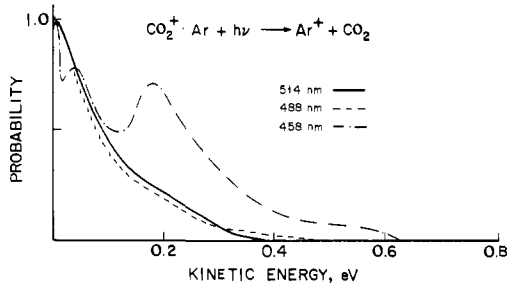

Figure 12. Kinetic energy release distributions for Ar^+ product ions at 514, 488, and 458 nm. Data points are eliminated for clarity.

from fragmentation on a repulsive surface and the lower energy feature from statistical vibrational predissociation. Two possible repulsive fragmentation pathways are shown in Figure 11. The problem with this explanation is that the kinetic energy of the higher energy features in Figure 12 does not substantially change with photon energy. Such a change would be expected if simple fragmentation from a repulsive surface were occurring.[12,13,19]

An alternative explanation is suggested when the data are plotted on a constant energy scale (Figure 13). Conservation of energy requires

$$h\nu - \Delta IP - KE = D_0^\circ(Ar\text{–}CO_2^+) + E_{INT}(CO_2) + E_{INT}(Ar^+) - E_{INT}(CO_2^+ \cdot Ar) \quad (6)$$

where $h\nu$ is the photon energy, ΔIP is the difference in ionization potentials of Ar and CO_2, KE is the product relative kinetic energy, $D_0^\circ(CO_2^+\text{–}Ar)$ is the binding energy of the CO_2^+·Ar cluster, $E_{INT}(Ar^+)$ is the internal energy carried off by the Ar^+ fragment, $E_{INT}(CO_2)$ is the internal energy carried off by the CO_2 photofragment, and $E_{INT}(CO_2^+ \cdot Ar)$ is the internal energy in the CO_2^+·Ar cluster before absorption of the photon. A percentage of the CO_2^+·Ar clusters has some internal excitation. This energy will lead to a broadening and shifting of the features observed in the kinetic energy distributions. However, to a first approximation we can ignore $E_{INT}(CO_2^+ \cdot Ar)$ for the purpose at hand. The value of $D_0^\circ(CO_2^+\text{–}Ar)$ is known, 0.26 eV.[18] There are several possibilities for the structure observed in Figure 13. First, the Ar^+ photofragment could be formed in the $^2P_{1/2}$ state, giving $E_{INT}(Ar^+) = 0.18$ eV. That possibility would explain the peak in the 514-nm curve at $h\nu - \Delta IP - KE = 0.43$ eV [$D_0^\circ(CO_2^+\text{–}Ar) + E_{INT}(Ar^+) = 0.26$ eV + 0.18 eV = 0.44 eV]. Such an explanation would not, however, account for the additional structure

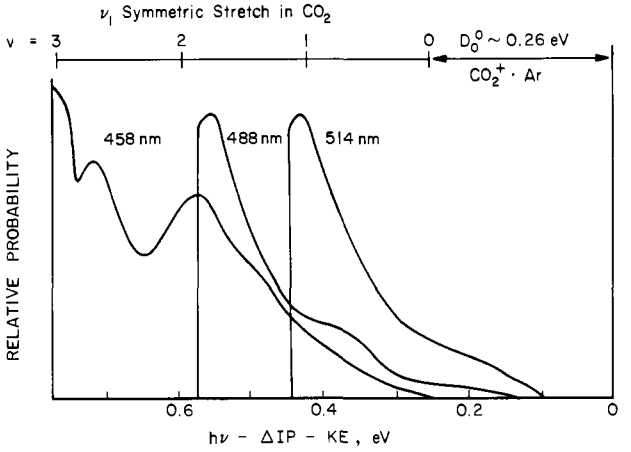

Figure 13. Plot of the Ar^+ kinetic energy distributions for photodissociation of CO_2^+·Ar at 514, 488, and 458 nm. The horizontal axis is plotted in energy units such that all three distributions are plotted on a common energy scale (see discussion in text following eq 6). Data points are eliminated for clarity.

Table I. Estimates of the CO_2 Product ν_1 Symmetric Stretch Vibrational State Distribution for Photodissociation of CO_2^+·Ar at the Indicated Wavelengths[a]

ν_1 vibrational state	wavelength, nm		
	514	488	458
$v = 0$	17	4	~0
$v = 1$	83	19	~0
$v = 2$	0	77	47
$v = 3$	0	0	53

[a] Integrated areas should be used for accurate determinations. However, due to the high degree of overlap of the features, peak heights were used. The data are probably accurate to ±30%.

seen in the 488- and 458-nm curves.

A second explanation is the structure is due to internal excitation of the CO_2 fragment. The CO_2 molecule has three normal modes: $h\nu_1 = 0.172$ eV (symmetric stretch), $h\nu_2 = 0.083$ eV (bend), and $h\nu_3 = 0.291$ eV (asymmetric stretch).[34] The features in Figure 13 cannot be fit by assuming sequential excitation in either ν_2 or ν_3.[35] However, all of the features can be nicely fit assuming sequential excitation of ν_1. The shoulder at ~0.26 eV would correspond to $v = 0$, the features at 0.43 eV to $v = 1$, the features near 0.58 eV to $v = 2$, and the feature near 0.74 eV to $v = 3$. Such an analysis indicates that the highest energetically accessible vibrational level in the CO_2 moiety is favored when CO_2^+·Ar absorbs a photon to form CO_2^+·Ar^{+*}. [A very similar circumstance holds for photodissociation of Kr·O_2^+ to form $Kr^+ + O_2$.[36] In that case the O_2 photofragment is formed preferentially in the highest accessible vibrational state allowed by conservation of energy ($v = 0$ for 514 nm, $v = 1$ for 488 nm, and $v = 2$ for 458 nm). There is no ambiguity about the assignment in the Kr·O_2^+ case since the $^2P_{1/2}$ state of Kr^+ is 0.67 eV above the $^2P_{3/2}$ state and O_2 has only a single vibrational mode.] A crude estimate of the branching ratios into the various vibrational levels of ν_1 for CO_2 can be made. These results are summarized in Table I.

The excitation of ν_1 in CO_2 is qualitatively supported by the photoelectron spectrum of CO_2.[37] In that spectrum the ν_1 mode of CO_2^+ is excited when the ion is formed by photon impact on

(34) Herzberg, G. "Electronic Spectra of Polyatomic Molecules"; van Nostrand Reinhold: New York, 1966.

(35) Actually, the sequence of features in Figure 13 could be accounted for by assuming ν_2 is excited in levels 0, 2, 4, and 6. There appears to be little reason why ν_2 would be excited two quanta at a time, however. It is also possible that ν_3 is excited to its 0, 1, 2, and 3 levels and that the CO_2 photofragment is highly rotationally excited. While this process seems unlikely it cannot be completely ruled out.

(36) Jarrold, M. F.; Misev, L.; Bowers, M. T. *J. Chem. Phys.* **1984**, *81*, 4369.

(37) Turner, D. W.; Baker, C.; Baker, A. D.; Brundle, C. R. "Molecular Photoelectron Spectroscopy"; Wiley-Interscience: London, 1970.

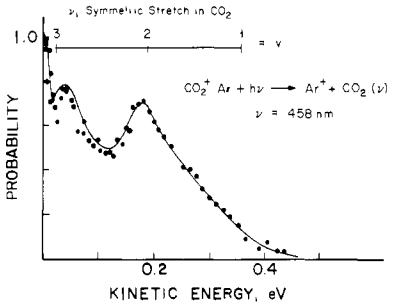

Figure 14. Plot of the Ar^+ kinetic energy distribution for photodissociation of $CO_2^+ \cdot Ar$ at 458 nm. The vibrational spacings for the ν_1 symmetric stretch of CO_2 are shown. The sharp feature near zero kinetic energy is presumably due to the tail of the $v = 4$ peak.

CO_2. The present case is more complicated due to the presence of the Ar atom and the fact that the reverse process is involved ($CO_2^+ \cdot Ar + h\nu \rightarrow CO_2 \cdot Ar^+$). This interpretation implies that the vibrational excitation of the CO_2 moiety occurs in the photon absorption process, not in the dissociation process—an interpretation consistent with the data presented here and with the $Kr \cdot O_2^+$ results previously discussed.

The CO_2 photofragment may be formed rotationally excited. The 458-nm Ar^+ kinetic energy distribution is replotted in Figure 14. Note that the separation between the $v = 3$ and $v = 2$ features is essentially equal to the experimental separation. (The signal to noise ratio in these experiments is low due to the extremely weak signal. As a consequence the precise separation between the features cannot be accurately determined. The following discussion and conclusions drawn from it should be viewed with this in mind.) A similar result is obtained from the 514- and 488-nm kinetic energy distributions, although in these cases the features are not as well resolved as they are in the 458-nm distribution. These results imply that the torque imparted to the CO_2 moiety in the fragmentation is small. A simple rigid rotor impulsive model[38] indicates that the average rotational energy in the CO_2 fragment should be

$$E_{ROT} = (\sin^2 \alpha)\left(1 - \frac{\mu_{BC}}{\mu_F}\right)E_{AV} \qquad (7)$$

where $180 - \alpha$ is the Ar–CO_2 bond angle, μ_{BC} is the reduced mass of the atoms at the end of the breaking bond, μ_F the reduced mass of the Ar^+/CO_2 fragments, and E_{AV} the energy available for partitioning into product rotation. In the limit of no rotational excitation $E_{ROT} = 0$. There are two ways that the right-hand side of eq 7 can be equal to zero: either $\mu_{BC} = \mu_F$ or $\alpha = 0°, 180°$. The equality $\mu_{BC} = \mu_F$ will occur only if the fragmenting Ar^+ ion interacts with the entire CO_2 molecule during dissociation. This could occur only for $\alpha = 90°$. Since dissociation into the Ar^+/CO_2 channel is fast relative to a rotational period for most product velocities (see Figure 8), the structure being probed is the $Ar \cdot CO_2^+$ structure as little or no rearrangement can take place before dissociation once the photon is absorbed. Hence, the two possible structures are

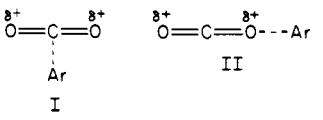

Of these two, structure I seems the more likely for two reasons. First, on electrostatic grounds the argon atom can interact with both of the positively charged oxygen atoms in structure I while in structure II it can only interact with one of them. Second, the lowest unoccupied molecular orbital (LUMO) on CO_2^+ is the nonbonding Π_g orbital. The individual lobes of this orbital are essentially perpendicular to the O=C=O axis and alternate in sign. Hence, this orbital provides no net overlap in the linear configuration with the highest occupied molecular orbital (HOMO) of argon, a p orbital. The p orbitals on argon can overlap to some extent with the LUMO of CO_2^+ in the perpendicular configuration although this overlap is probably small and the interaction weak. This analysis would suggest the dominant interaction between CO_2^+ and Ar is electrostatic, and structure I is favored. This result is in contrast to the results for $Kr \cdot O_2^+$ where substantial rotational excitation of the O_2 photofragment was observed.[36] In that case it was inferred that $\alpha \simeq 135°$ and LUMO/HOMO interactions dominated over the electrostatic interactions.

If the breakup of the nascent photoexcited $CO_2 \cdot Ar^+$ cluster were strongly impulsive, then structure I would predict the CO_2 bending mode ν_2 might be excited and structure II would predict the asymmetric stretch ν_3 might be excited. In fact the ν_1 symmetric stretch appears to be the CO_2 mode excited in the photodissociation event. This suggests that the excitation of the CO_2 moiety occurs in the photoabsorption process and not in the dissociation process and that the repulsive $CO_2 \cdot Ar^+$ surface is relatively flat along the coordinate that leads to Ar^+/CO_2 products.

The reaction labeled c in Figure 11 leads to formation of CO_2^+/Ar products. The kinetic energy release distribution for this process is peaked away from zero kinetic energy (Figure 6), indicating that either a large reverse activation barrier or a repulsive surface is involved. A reverse activation energy can be ruled out since CO_2^+ readily associates with Ar at thermal energies. Electronic predissociation between the $CO_2 \cdot Ar^+$ bound surface and the repulsive surface correlating with CO_2^+/Ar products is, however, very probable. The 0° and 90° peak shapes for CO_2^+ formation suggest that fragmentation of $Ar^+ \cdot CO_2^*$ takes place on a time scale which is long compared to molecular rotation. An electronic predissociation mechanism would account for the slow step. These ions have sufficient energy to vibrationally predissociate to form Ar^+/CO_2 even for the lowest energy photons [E_{AV}(514 nm) = 0.18 eV]. Hence, a competition between vibrational predissociation and electronic predissociation is occurring. Unfortunately we cannot obtain the percentage of the Ar^+ product that comes from vibrational predissociation and that that comes from direct dissociation of the repulsive state. It appears likely that some of the Ar^+ ions do come from vibrational predissociation, at least at 514 nm. The bulk of them appear to come from direct dissociation on the repulsive curves, however, if the analysis presented earlier in this section is correct.

Comparison with the Charge-Transfer Reaction. The charge-transfer reaction

$$Ar^+ + CO_2 \rightleftarrows [Ar^+ \cdot CO_2]^* \rightarrow CO_2^+ + Ar \qquad (1)$$

proceeds at about 50% efficiency.[15] If the reaction proceeds through a collision complex, then at thermal energies vibrational predissociation to form Ar^+/CO_2 is in competition with electronic predissociation to form CO_2^+/Ar. At the lowest photon energy (2.41 eV or 514 nm) it appears that the lifetime of the $CO_2 \cdot Ar^{+*}$ bound complex that leads to CO_2^+ product is of the order of a rotational period or longer ($\sim 1\text{–}5 \times 10^{-12}$ s). This is a reasonable lifetime for vibrational predissociation of a small species like $CO_2 \cdot Ar^+$ with less than 0.2 eV excess energy. Little is known about electronic predissociation in such systems. The lifetime of the comparable complex formed by Ar^+/CO_2 collision will be longer because the excess energy is less (~ 0.03 eV). This fact no doubt contributes to the greater probability for forming CO_2^+/Ar product by charge transfer than by photodissociation of $CO_2^+ \cdot Ar$. At the higher energies used in the photodissociation experiment (488 and 458 nm) the probability of forming CO_2^+/Ar products decreases significantly (see Figure 4). This occurs for two reasons. First, in the photodissociation experiments the $CO_2 \cdot Ar^{+*}$ species is probably being preferentially formed on a repulsive surface that leads directly to Ar^+/CO_2 products as photon energy increases. Hence the percentage of $CO_2 \cdot Ar^{+*}$ species formed in the bound state decreases, yielding a smaller CO_2^+/Ar product yield. Second, at higher energies the vibrational predissociation rate of bound $Ar^+ \cdot CO_2^*$ (to form $Ar^+ + CO_2$) will probably increase faster than the electronic predissociation rate (to form $CO_2^+ + Ar$) although there is no direct experimental

(38) Busch, G. E.; Wilson, K. R. *J. Chem. Phys.* **1972**, *56*, 3626.

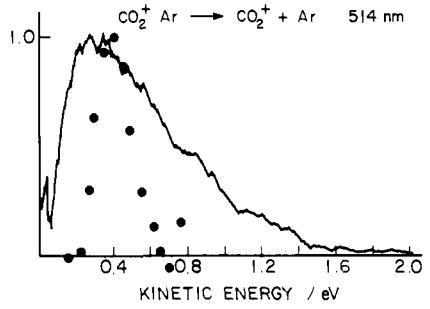

Figure 15. Plots of the kinetic energy distributions of the CO_2^+ product from both the photodissociation of CO_2^+·Ar (this work) and from the Ar^+/CO_2 charge-transfer reaction (ref 16). The points are for the charge-transfer reaction, and the line for photodissociation.

evidence to support this suggestion.

It does appear that CO_2^+/Ar products are formed by the same mechanism regardless of whether CO_2·Ar^{+*} is formed by ion–molecule reaction or photoexcitation of CO_2^+·Ar. This suggestion is supported by the data in Figure 15. In this figure the CO_2^+ kinetic energy distributions from both photoexcitation of CO_2^+·Ar and the charge-transfer reaction (eq 1) are given.[16,39] Both distributions are very similar, peaking at about 0.4 eV. It is not surprising that they differ to some extent given the very different experimental procedures used and the somewhat different energy and angular momentum distributions of the excited CO_2·Ar^{+*} ions. Since the photodissociation process must proceed via an intimate CO_2·Ar^{+*} complex, the implication is that the charge-transfer reaction also does and such long-range processes as electron jump are not important in this case.

Summary and Conclusions

(1) Photodissociation of CO_2^+·Ar results in two product ions, CO_2^+ and Ar^+. The fraction of CO_2^+ formed varies from ~5% at 458 nm to ~14% at 514 nm. This result is in qualitative agreement with the bimolecular charge-transfer reaction

$$Ar^+ + CO_2 \rightarrow CO_2^+ + Ar$$

which shows a decrease in the rate constant with increasing Ar^+ kinetic energy.[15b] The similarities of the present photodissociation study and the charge-transfer reaction are presented.

(2) The total photodissociation cross section is approximately constant at 11×10^{-18} cm^2 over the wavelength range studied.

(3) Kinetic energy release distributions for production of Ar^+ are bimodal. The 0° and 90° peak shapes indicated that Ar^+ is produced by two mechanisms, one which is fast and the other slow relative to the rotational time scale. We propose that the slow pathway is due to statistical decomposition of a bound CO_2·Ar^+ cluster ion and is a minor process while the fast pathway is the result of direct fragmentation from a repulsive surface and is the major process.

(4) The kinetic energy distributions are consistent with the fast process forming the CO_2 photofragments vibrationally excited in the ν_1 symmetric stretch. The highest level allowed by conservation of energy is formed at all photon energies. The CO_2 neutral fragment has little rotational energy, suggesting a T-shaped or linear CO_2^+·Ar complex, although a slightly nonlinear complex cannot be ruled out.

(5) The kinetic energy release distribution and 0° and 90° peak shapes for CO_2^+ show that CO_2^+ is formed via a slow mechanism with a large kinetic energy release. The kinetic energy release distribution is peaked at ~0.4 eV. These observations are consistent with electronic predissociation of a bound CO_2·Ar^+ surface to a repulsive surface leading to ground-state CO_2^+/Ar products.

Acknowledgment. We gratefully acknowledge the support of the Air Force Office of Scientific Research under Grant AFOSR-82-0035 and the National Science Foundation under Grant CHE80-20464.

Registry No. Co_2^+, 12181-61-2; Ar^+, 14791-69-6.

(39) O'Keefe, A.; Parent, D.; Bowers, M. T., unpublished data.

Structure Revision of the Antibiotic Pulvomycin

Richard J. Smith,[†] Dudley H. Williams,*[†] Jennifer C. J. Barna,[†] Ian R. McDermott,[‡] Klaus D. Haegele,[‡] Francois Piriou,[‡] Joseph Wagner,[‡] and William Higgins[‡]

Contribution from the University Chemical Laboratories, Cambridge, United Kingdom CB2 1EW, and Merrell Dow Research Institute, 67084 Strasbourg, France.
Received October 15, 1984

Abstract: The hitherto accepted structure of the antibiotic pulvomycin (also known as labilomycin) (**1**) has been shown to be incorrect. Fast atom bombardment mass spectrometry has shown pulvomycin to have a molecular weight of 838, and high field NMR experiments have allowed the structure **2** to be deduced. Pulvomycin, which inhibits prokaryotic protein biosynthesis by binding to prokaryotic elongation factor Tu, has been shown by this study to possess a triene system, two trienone systems, and an unusual 22-membered lactone ring. It also contains one sugar unit, labilose, the previously deduced stereochemistry of which has been confirmed. The relative stereochemistries of six of the eight chiral centers in the aglycone have been established by NMR studies, and the ^{13}C NMR spectrum of pulvomycin has been almost completely assigned by use of a two-dimensional heteronuclear chemical shift correlation experiment.

The antibiotic pulvomycin was first reported in 1957[1] and was subsequently "rediscovered" in 1963[2] and its structure determined.[3] The latter isolate was named labilomycin because of its extreme lability but was subsequently shown by Tishler's group[4] to be identical with pulvomycin. The comparison was based on UV and IR spectral data, pulvomycin having a very characteristic UV

[†] University of Cambridge.
[‡] Merrell Dow Research Institute.

(1) Zief, M.; Woodside, R.; Schmitz, H. *Antibiotic Chemother. (Basel, 1954—70)* **1957**, *7*, 384–386.
(2) Akita, E.; Maeda, K.; Umezawa, H. *J. Antibiot., Ser. A.* **1963**, *16*, 147–151.

0002-7863/85/1507-2849$01.50/0